ENGINEERING Biomass
https://doi.org/10.2738/ENGB.2026.0002

Original Research

Wood Woundplast for High-efficiency Chronic Wounds Healing

Yingying Liu[1*], Jianfu Tang[1*], Wenqi Dong[2*], Yueying Zhang[1], Zixuan Yang[1], Ruihao Zhang[1], Ran Yin[1], Shilong Yang (✉)[2], Wentao Gan (✉)[1], Jian Li (✉)[1]

1 Key Laboratory of Bio-based Material Science & Technology (Ministry of Education), Northeast Forestry University, Harbin 150040, China
2 College of Wildlife and Protected Area, Northeast Forestry University, Harbin 150040, China

GRAPHICAL ABSTRACT

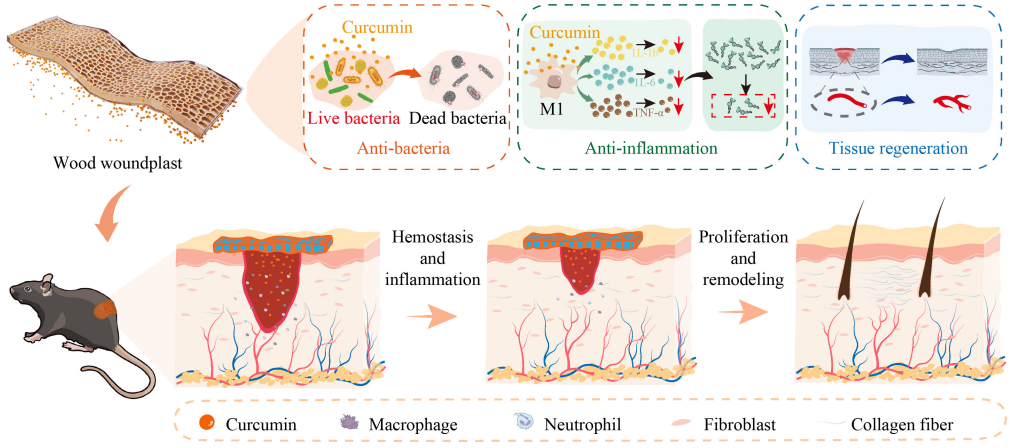

HIGHLIGHTS

- A wood woundplast was prepared by polyvinyl alcohol and curcumin modification.
- The WH-1000 exhibited high stretchability and fatigue resistance over 300 cycles.
- Wood woundplast showed excellent antibacterial and anti-inflammatory effects.
- Animal experiments demonstrated accelerated wound healing of wood woundplast.

ABSTRACT The healing of chronic wounds is a global issue that poses a serious threat to public health and healthcare. Biopolymer materials are non-toxic and biocompatible dressings, however, the lack of antimicrobial properties limits their clinical application. This work adopts a top-down approach, utilizing the porous structure of natural wood and the high-water content of polyvinyl alcohol (PVA) to prepare a flexible wood woundplast containing curcumin. The wood woundplast resolves inherent limitations of traditional dressings, including wound adherence and rapid release, by offering a moisture-retentive environment and sustained release. The dressing exhibits excellent tensile performance, with a tensile strain of up to 270% and the ability to withstand 300 cycles of tensile stress without damage, due to the strong hydrogen bonding between the cellulose in wood and PVA. Moreover, it can absorb wound exudate to facilitate moisture exchange while releasing curcumin. Benefiting from the ability of curcumin to disrupt bacterial cell membranes and inhibit the transcription of inflammatory factors, the wood woundplast possesses dual antimicrobial and anti-inflammatory functions. The wood-based woundplast provides good biocompatibility, uses abundant raw materials, and allows flexible manufacturing, representing an effective dressing to accelerate wound healing.

Received 24 Apr 2026; accepted 22 May 2026

E-mails: syang2020@nefu.edu.cn (Yang S.),
wtgan@nefu.edu.cn (Gan W.),
nefulijian@163.com (Li J.).

* These authors contributed equally to this work.

KEYWORDS Deep eutectic solvent; Wood hydrogel; Curcumin; Antibacterial and anti-inflammatory; Wound healing

1 Introduction

Chronic wounds [1], including infected wounds, burns and diabetic foot ulcers, have become a major challenge for healthcare systems worldwide due to their complex healing mechanisms, high risk of infection, and persistent inflammatory response [2,3]. Chronic wounds are often associated with bacterial biofilm formation and persistent inflammation [4–7]. These pathological features severely impede the wound healing process by disrupting the four critical phases, including haemostasis, inflammation, proliferation, and remodelling, which not only prolong the duration of the inflammation but also compromise tissue structure and cellular functions [8–11]. Traditional dressings, including gauze, vaseline gauze, and synthetic fiber cloth, are inexpensive and readily available but hinder chronic wound healing [12,13]. For example, gauze absorbs blood and adheres to the wounds as blood coagulates, causing secondary bleeding and pain upon removal. The insufficient adhesive strength requires additional dressings for wound, making it difficult to meet the specific needs of chronic wound security [14]. Biopolymer-based dressings materials, including chitosan [15], alginate [16], and collagen [17], offer excellent biocompatibility, high affinity for human tissues, good degradability, and gradual metabolism and absorption *in vivo*, thus avoiding long-term residuals. Among them, bacterial cellulose promotes rapid chronic wound healing through its natural extracellular matrix protofibril structure, which ensures high cell adhesion and outstanding water retention. However, its widespread adoption is limited by difficulties in fabrication and low production yields. Based on these limitations, the development of efficient and multifunctional wound dressings is important in biomedical applications.

Wood, an abundant and renewable resource, is an ideal substrate with a three-dimensional (3D) porous structure for the biomedical applications due to its hierarchical porous structure, good mechanical properties, and biocompatibility [19–22]. Wood-derived cellulose nanofibers (CNF) exhibit superior features in promoting wound healing and tissue regeneration. Nevertheless, processing CNF in a bottom-up approach requires the disassembly of the wood cell walls by energy-intensive and long-period production, including acidification, catalytic oxidation, and high-pressure homogenization [23,24]. In contrast, a top-down approach achieved through simple delignification methods preserves the 3D wood structure conducive to exudate absorption while delivering exceptional flexibility and adaptability. Recently, Luan et al. [25] successfully developed a pH-responsive “wooden scroll” nutrient delivery system for targeted delivery of enteral nutrients. Huang et al. [26] engineered a flexible wood dressing functionalized with aggregation-induced emission photosensitizer, which significantly enhanced the infected wounds healing through combined photodynamic therapy and moisture management. Our previous study prepared magnetized wood as a soft robot for targeted cargo transportation [27]. However, these methods all rely on external control measures, such as pH regulation, applied magnetic fields, and photodynamic effects. Although they employ a top-down approach to material preparation, the methods they use for wood delignification shows adverse environmental impacts. In contrast to other pretreat methods, deep eutectic solvents (DES) present distinct advantages as an emerging green solvent for wood pretreatment. Unlike the acidic sodium chlorite method, DES processing does not generate harmful gases such as chlorine. In comparison to the sodium sulfite and sodium hydroxide process, it avoids the use of highly corrosive strong alkalis. Furthermore, DES is recyclable, thereby minimizing environmental pollution, and offers additional benefits including low cost, low toxicity, and simple preparation [28,29].

To optimize wound healing outcomes and enhance therapeutic efficacy, the active pharmaceutical compounds are always incorporated into various carrier materials [30–33]. Conventional antibiotics, such as beta-lactams [34], macrolides [35], and aminoglycosides [36], are often used to combat the bacterial infestation and inflammation during chronic wound healing. Research has demonstrated that the overuse of antibiotics may increase bacterial resistance [37]. Moreover, since antibiotics typically target only specific bacteria, they struggle to address the complex microbiological environment in chronic wounds [38]. In contrast, plant-derived medicines have begun to attract the attention of researchers, such as tea polyphenols, honeysuckle extracts, curcumin and so on. Plant-derived [39,40] medicines show notable advantages of environmental sustainability, biocompatibility, and a favorable safety profile with minimal side effects. Curcumin [41], a polyphenolic compound from turmeric rhizomes, offers superior broad-spectrum antibacterial, anti-inflammatory, antioxidant, and wound healing properties [42,43]. It effectively reduces the inflammatory response to wounds and promotes angiogenesis and collagen deposition, thereby accelerating wound healing [44]. Based on the natural microchannel structure and high biocompatibility of wood, can achieve drug storage, protection, and

precise controlled release, making them a promising biopharmaceutical carrier material.

In this study, we developed a flexible wood woundplast composed of wood hydrogel loaded with curcumin particles. This dressing exhibits both antimicrobial and anti-inflammatory properties while effectively accelerating wound healing. We utilize the cross-sectional wood and curcumin as raw materials, both of which are characterized by their green and sustainable properties. We first treated the wood with a deep eutectic solvent (DES) of choline chloride and lactic acid to partially remove lignin and hemicellulose. This treatment exposed active hydroxyl groups in the cell walls, proving additional binding sites for curcumin and polyvinyl alcohol (PVA). The 3D porous structure of wood served as a supporting framework for the PVA hydrogel. The inherent porous architecture of wood, with its open and straight-through cell lumina, provides an ideal environment for curcumin loading and release. Hydrogen bond networks form among cellulose, polyvinyl alcohol (PVA), and curcumin [45,46]. Following cross-linking PVA into the wood structure not only can accelerate the wound exudate absorption but also enables the release of curcumin molecules through the water exchange process. The high-water content of PVA maintains a moist wound environment, thereby preventing secondary bleeding caused by drying and adhesion. Furthermore, the wood woundplast possesses excellent flexibility, enabling a close fit to skin surfaces and articulated areas such as joints. The slowly released curcumin molecules effectively penetrate the biofilm barrier to the wound tissue. Owing to the excellent antimicrobial performances of curcumin, the wood woundplast effectively inhibits the growth of common pathogenic bacteria (including *Escherichia coli*, *Staphylococcus aureus*, and *Pseudomonas aeruginosa*). Additionally, wood woundplast shows excellent anti-inflammatory effects by significantly reducing both M1-type macrophage activation and pro-inflammatory factor production. With its ability to support nutrient and oxygen delivery, the wood woundplast promotes cell proliferation and migration while increasing the expression of pro-angiogenic factors, which significantly accelerates wound healing and tissue regeneration (Fig. 1A, B). Wood woundplast leverages the natural porous structure of wood and the network structure of PVA to successfully achieve the loading and controlled release of curcumin particles. Combining biocompatible wood, flexible PVA, and natural curcumin, the wood woundplast represents a simple and efficient biomedical dressing for chronic

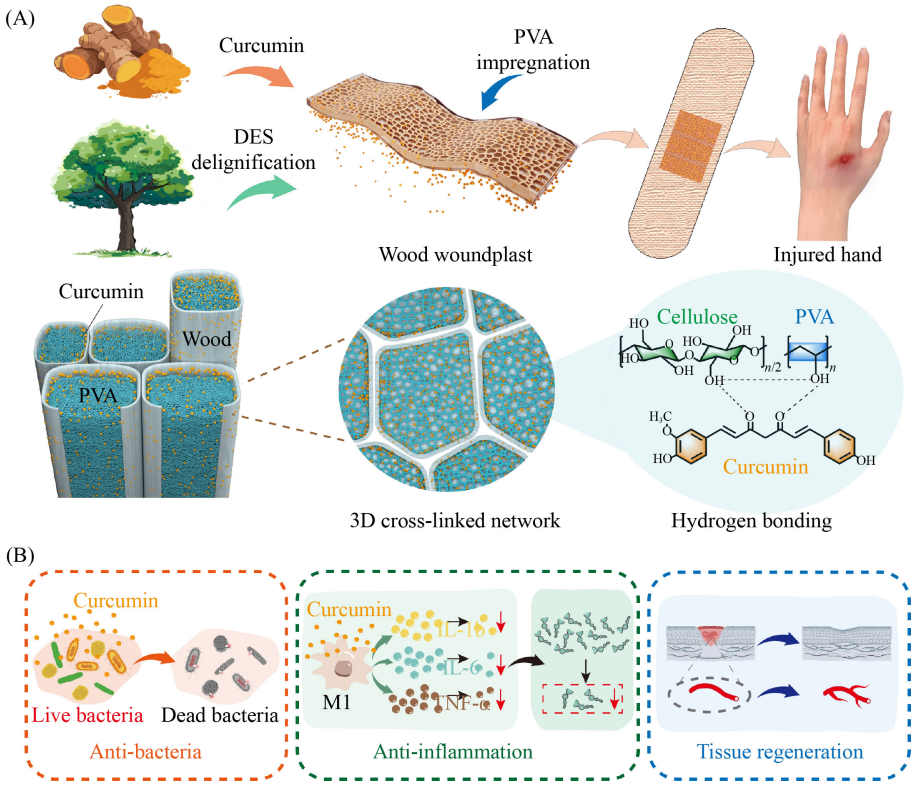

Fig. 1 Preparation of wood woundplast. (A) The schematic of the material microstructure. (B) The chronic wound healing mechanism includes antibacterial action, inflammatory reduction, and tissue regeneration.

wound healing, showing great potential in chronic wound care applications.

2 Experimental Section

2.1 Materials and chemicals

The balsa wood used in this experiment was purchased from a local sawmill in Heilongjiang Province. The dimensions of the balsa wood were 60 mm × 30 mm × 500 μm (longitudinal × radial × tangential). Curcumin [molecular weight (MW): 368.38], choline chloride (MW: 139.62), and polyvinyl alcohol [polymerisation degree: 1799, alcoholysis degree: 98%–99% (mol/mol)], were all purchased from Shanghai McLean Bio-Chemical Technology Co., Ltd. Sodium chloride, sodium hydroxide, and lactic acid were purchased from Tianjin Tianli Chemical Reagents Co., Ltd. All chemicals were of analytical grade purity and used as received, without further purification.

2.2 Preparation of wood woundplast

First, a deep eutectic solvent (DES) was prepared with a molar ratio of choline chloride to lactic acid of 1:10. Cross-sectional samples of balsa wood were immersed in the DES solution and treated in an oil bath at 90 °C for 2 h. The DES-treated wood was then thoroughly washed with deionized water and freeze-dried. Secondly, curcumin was dissolved in dimethyl sulfoxide (DMSO) solution (1000 μg·ml^{-1}). The freeze-dried wood is immersed in the curcumin solution for 30 min, rinsed with deionized water to remove excess solution, and freeze-dried again. Subsequently, the wood was immersed in a 10 wt% PVA solution for 6 h to allow PVA to infiltrate the wood cell cavities and intercellular spaces. The sample was then placed in a freezer for 2 h to set the shape. Following this, the wood was immersed in a mixture of NaOH and NaCl (1:1 by volume) to facilitate cross-linking. Finally, the sample was neutralized in an acetic acid solution (pH = 5), rinsed with deionized water until a neutral pH was achieved, resulting in a flexible curcumin-loaded wood hydrogel.

2.3 Characterization

The structural changes of the material during tensile loading were characterized using an optical microscope (MeiMei, MJ31). The microstructure of the material was characterized using a scanning electron microscope (SEM, HITACHI TM3030). The three-dimensional structure of the material was scanned using a high-resolution 3D X-ray microtomography system (Micro-CT, SKYSCAN I273), distinguishing structural features through density variations. The change in functional groups of samples was investigated and analyzed using a Fourier transform infrared (FTIR) spectrometer (Thermo Scientific Nicolet iN10) on the wavelength range between 400 cm^{-1} and 4000 cm^{-1}, and with a resolution of 0.5 cm^{-1}, over 32 scans. The variations of the crystal structure in as-prepared samples were characterized and calculated through X-ray scattering (XRD; X, Pert3 Powder) at a scan rate of 5° min^{-1} and 2θ degree range between 5° and 50°. The absorption spectrum was characterized using a ultraviolet-visible (UV-Vis) spectrometer over a wavelength range of 300–600 nm to evaluate its optical properties. The mechanical tensile and cyclic tests of prepared samples were performed on a universal testing machine (Suns, UTM2503) with a loading speed of 1 mm·min^{-1}.

2.4 Antibacterial test

The antibacterial activity of flexible wood hydrogels containing different concentrations of curcumin was evaluated against *Staphylococcus aureus*, *Escherichia coli*, and *Pseudomonas aeruginosa* using the zone of inhibition method. Bacteria suspensions were diluted to a concentration of 1 × 10^3 colony-forming units (CFU) mL^{-1}, and 50 μL aliquots were inoculated onto Luria-Bertani (LB) agar plates. Samples with a diameter of 11 mm were aseptically placed on the inoculated agar and incubated at 37 °C for 24 h. After incubation, the inhibition zones were photographed, and their diameters were measured to quantify antibacterial activity.

2.5 Cytotoxicity test

RAW264.7 cells were seeded into a 96-well plate at a volume of 100 μL per well, and cultured in a 5% CO_2 incubator for 24 h. Subsequently, the extracts of Cur, PVA, Cur/PVA, and WH-100 were introduced to the respective wells, followed by another 24 h of incubation. Then, added 10 μL of CCK-8 solution and continued incubation for 4 h. The absorbance at 450 nm was measured using a microplate reader, and the cell viability rate was calculated based on the formula in the manual.

2.6 *In vitro* anti-inflammatory test

To evaluate the anti-inflammatory effects of wood wounds, RAW264.7 cells were seeded in a six-well plate and exposed to 10 μg·mL^{-1} lipopolysaccharide (LPS). The cells were randomly assigned to different treatment groups and incubated for 48 h with extracts of no

material (control), LPS alone, Cur, Cur/PVA, and WH-1000. Following incubation, mRNA was extracted from each group, reverse-transcribed into cDNA, and the mRNA expression levels of IL-1β, TNF-α, and IL-6 were quantified using quantitative real-time PCR. *GAPDH* was used as a housekeeping gene.

2.7 Establishment of a chronic wound model and assessment of wound healing

A back wound model was established in C57L/6 mice (8 weeks old). After anaesthetization, the dorsal surface of each mouse was depilated using depilatory cream and disinfected alternately with iodine and alcohol three times. A full-thickness wound with a diameter of 6 mm was subsequently created on the back. The mice were randomly divided into three experimental groups: control, WH, and WH-1000. Wound areas were photographed and documented on days 0, 3, 7, 9, 11, and 14 post-wounding for further quantitative analysis.

2.8 H&E staining and paraffin sections

On days 7 and 14 of treatment, mice were euthanised, and skin tissue samples were removed from the wound area. The collected tissues were rinsed with saline, fixed in 4% paraformaldehyde for 24 h, and subsequently dehydrated, embedded in paraffin, and sectioned. The sections were then stained with hematoxylin and eosin (H&E), and imaged for histological analysis.

3 Results and Discussion

3.1 Preparation and microstructure of wood woundplast

To enhance the loading and releasing of curcumin particles, transverse sections of wood chips (500 μm thick) are cut. Scanning electron microscopy (SEM) images of the natural wood along the transverse section reveal its characteristic hierarchical and porous structure, showing the axially aligned vessel and fibre elements. SEM images of the wood radial section reveal a structure of numerous hollow fiber cells. These cells are neatly aligned along the trunk axis, establishing an array of continuous longitudinal microchannels. This natural microporous scaffold, composed of these open lumens, makes it well-suited for the efficient loading and transport of particles (Fig. 2A–C and Fig. S1). Despite the advantage of high particle loading offered by the 3D porous structure, the inherent rigidity of natural wood poses a significant challenge in biomedical applications due to its brittleness under deformation. Deep eutectic solvent (DES) treated wood (Fig. 2D) can break hydrogen bonding networks between cellulose, lignin, and hemicellulose in wood, thereby improving its softness. DES treated wood exhibits wrinkled cell walls (Fig. 2E), surface grooves (Fig. S2), wood cells are arranged in a regular pattern (Fig. 2F). After DES treatment, the specific surface area from 0.7777 $m^2 \cdot g^{-1}$ to 1.1672 $m^2 \cdot g^{-1}$ (Fig. S3), demonstrating enhanced porosity. This is because the DES treatment results in the partial removal of lignin and hemicellulose, which increases the specific surface area of the wood, thereby leading to an increase in porosity. The relative content of hemicellulose and lignin decreases from 25.78% to 18.01% and 22.16% to 16.57%, respectively, while the relative content of cellulose significantly increases from 46.66% to 61.51% (Fig. S4). When immersed in curcumin solution for 30 min, the DES treated wood rapidly adsorbs curcumin molecules onto the wood cell wall (Fig. S5). This adsorption occurs through hydrogen bonds between the hydroxyl groups of the curcumin and those in cellulose exposed on the wood cell wall surface. We further developed the wood woundplast by impregnating DES treated wood with biocompatible PVA. As shown in Figure 2G–I, the impregnation of PVA resin filled the wood cellular lumens, which caused the collapsed cell walls to swell and restored them to a full state. Furthermore, the PVA penetrated the intercellular spaces, forming a continuous 3D network that consolidated the entire wooden framework.

In the Fourier transform infrared (FTIR) spectra, the absorption peak at 3333 cm^{-1} representing the O–H stretching vibration exhibits a significant broadening, attributed to the partial removal of the lignin and hemicellulose after DES treatment. The persistence of the C–O stretching vibration peak at 1032 cm^{-1}, with no significant shift or intensity change, confirms that the cellulose remains chemically unchanged after DES treatment (Fig. 2J). The increased surface hydroxyl groups provide additional active sites for curcumin particle loading through hydrogen bonding. Moreover, the delignification preserves the crystal structure of cellulose nanofibers in wood, as evidenced by characteristic peaks attributed to cellulose crystal (110) and (200) plane diffraction peaks appearing near $2\theta = 16°$ and 22.3° in the XRD spectra. In the XRD spectra of wood woundplast, cellulose crystal (110) and (200) plane diffraction peaks appear near $2\theta = 16°$ and 22.3°, while the characteristic plane diffraction peak of PVA appears near $2\theta = 20°$. The coexistence of the characteristic peaks from cellulose and PVA in the wood woundplast indicates the formation of a cross-linked network (Fig. S6). To further investigate the microstructure of the wood woundplast, a high-resolution 3D X-ray microimaging

https://doi.org/10.2738/ENGB.2026.0002

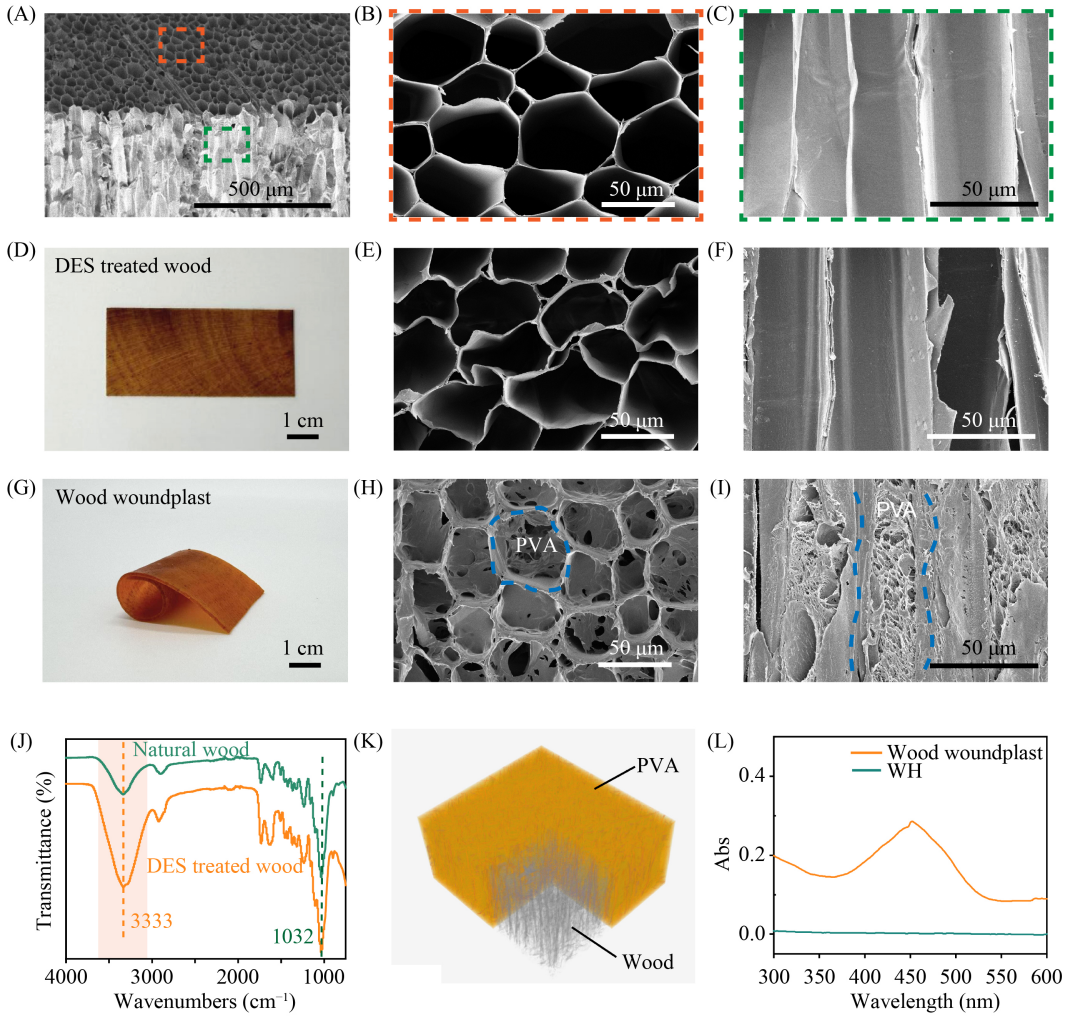

Fig. 2 Morphological characterization of wood woundplast. (A) SEM image of natural wood. (B) Cross-sectional SEM image of natural wood, showing its natural porous structure. (C) SEM image of natural wood along the longitudinal direction demonstrates the vertically aligned wood fibers. (D) Photograph of DES treated wood. (E) Cross-sectional SEM image of DES treated wood, showing the shrinkage of the cell wall. (F) Longitudinal SEM image of DES treated wood. (G–I) Photograph, cross-sectional and longitudinal SEM images of wood woundplast, showing the flexibility after PVA filling. (J) FTIR spectra of natural wood and DES treated wood, showing the strong O–H vibration absorption peak after DES treatment. (K) Micro-CT image of wood woundplast, showing that the PVA fills the wood cell lumens. (L) UV absorption spectra of wood hydrogel (WH) and wood woundplast, showing successful release of curcumin.

system demonstrates that wood serves as the skeleton of the wound dressing, while PVA functions as a flexible filler that encapsulates both the wood and curcumin (Fig. 2K). In this 3D structure, wood serves as the skeleton of the wound dressing, while PVA functions as a flexible filler that encapsulates both the wood and curcumin. This design provides flexibility that allows for the wound dressing to adapt to various deformation conditions. The wood hydrogel maintains the porous structure of the wood (Fig. S7), providing sufficient spaces for the active curcumin molecule release. UV-Vis spectroscopy of aqueous leachates from immersed wood woundplast confirmed the efficient curcumin release within the wood porous structure (Fig. 2L), demonstrating potential applications as a pharmaceutical excipient.

3.2 Mechanical properties of wood woundplast

The wood skeleton provides good mechanical properties for the wood woundplast. The natural wood exhibits a tensile strength of 0.688 MPa and a tensile strain of 0.95%. After DES treatment, these values change to 0.541 MPa and 4.96%, respectively. The decrease in strength can be attributed to the partial breakdown of hydrogen bonds among cellulose, lignin, and hemicellulose within the wood microstructure. In comparison, the PVA hydrogel shows a lower tensile

strength of 0.060 MPa but an exceptionally high tensile strain of 211.28% (Fig. S8). By combining PVA with the DES-treated wood scaffold, we obtain a wood woundplast composite that effectively balances flexibility and strength. This composite achieves a tensile strength of 0.684 MPa and an elongation at break of 270%, which is a 26.43% increase and a remarkable 54.44-time improvement over those of DES treated wood, respectively (Fig. 3A), demonstrating the synergistic effect of the wood skeleton and the PVA matrix. The enhanced mechanical properties of wood woundplast originate from the robust hydrogen bonding and van der Waals forces between cellulose nanofibers and PVA chains at wood-polymer interfaces. The fracture energy of wood woundplast (1.258 MJ·m^{-3}) is 26 times greater than that of pure PVA hydrogel (0.048 MJ·m^{-3}) (Fig. 3B), demonstrating the exceptional toughness. To prove the energy dissipation mechanism, we performed successive loading-unloading tensile tests at increasing strain levels (20% to 100%). The results clearly show that as the tensile strain increased from 20% to 100%, the hysteresis loops of the wood hydrogel samples become more pronounced (Fig. 3C). Progressive enlargement of hysteresis loops (Fig. 3C) and rise in energy loss coefficient from 0.157 to 0.464 confirm strain-dependent energy dissipation, with hydrogen bonds acting as sacrificial bonds. Successive tensile cycling (300 cycles at 100% strain) reveals dynamic fatigue behavior. Initial high energy dissipation (cycle 1: energy loss coefficient = 0.237) decreases during subsequent cycles, followed by a slight recovery in energy loss coefficient after 200 cycles (Fig. 3D). The non-monotonic dissipation pattern suggests a progressive reorganization of hydrogen bond networks rather than irreversible structural damage. The material maintained its structural integrity throughout testing, demonstrating excellent fatigue resistance with stable hysteresis after 300 cycles. Wood woundplast also demonstrates remarkable flexibility, enabling complex shape transformations such as stretched knots and curled ribbons without breaking (Fig. 3E, F). This exceptional deformability maintains the structural integrity even when subjected to multiaxial stresses.

To further investigate the structural changes of wood woundplast during tensile deformation, we photographed its morphological changes. PVA fills the cell lumens and intercellular spaces of wood woundplast, where the wood

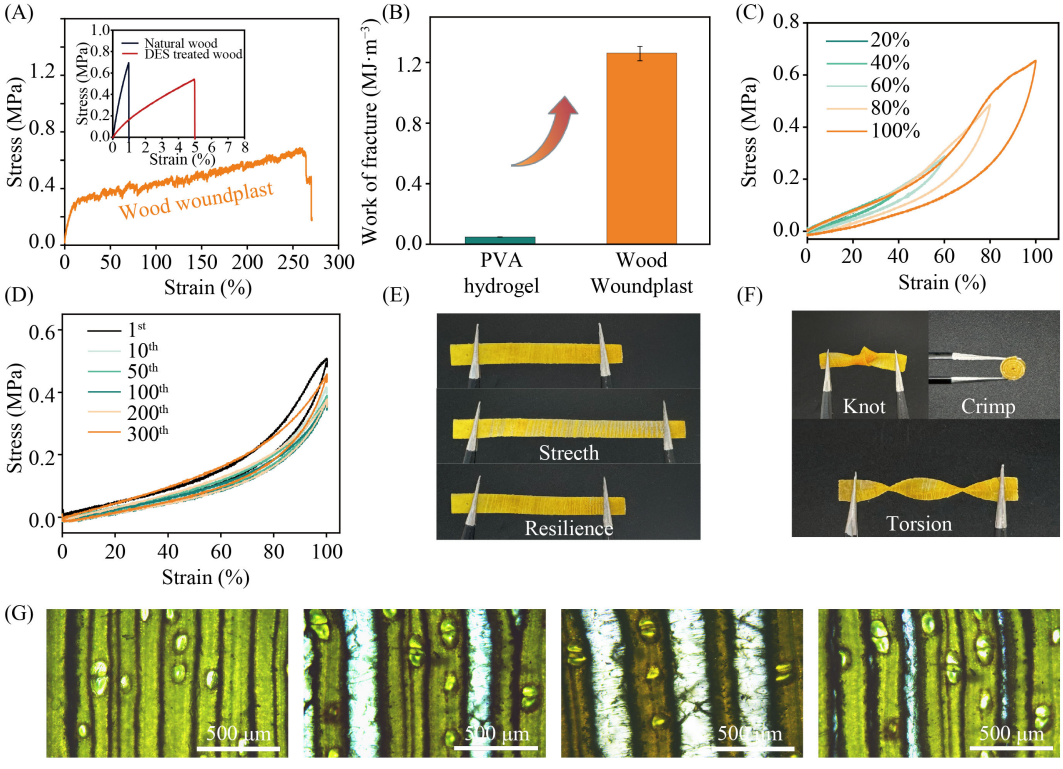

Fig. 3 Mechanical properties of wood woundplast. (A) Stress-strain curves of natural wood, DES treated wood and wood woundplast, showing the good tensile strength and tensile strain of wood woundplast. (B) Fracture work of PVA and wood woundplast, indicating the toughness of wood woundplast. Cyclic tensile tests of the wood woundplast at different strains (C) and cycle numbers (D), showing the good fatigue resistance. (E) Tensile rebound performances and (F) flexibility of wood woundplast. (G) The optical images of tensile resilience of wood woundplast, showing its deformation during the stretching and rebound.

cells are arranged in a regular pattern. When natural wood experiences tensile stress, its cell walls flatten into hexagonal configuration, and wood rays suffer irreversible fracture. In contrast, the wood woundplast remains intact under identical loading conditions. This fracture resistance arises from the hydrogen bonding network between PVA chains and cellulose molecules, which effectively counteracts applied tensile force. Unlike the weak hydrogen bonds between cellulose molecules that fracture under the same tensile stress, the wood woundplast demonstrates significant elastic recovery. When tensile stress is removed, it returns to its original shape with minimal permanent deformation. This superior resilience stems from the strong hydrogen bonds formed within the PVA-cellulose network (Fig. 3G).

3.3 Antibacterial, anti-inflammatory and cytotoxic effects

Chronic wounds are often colonized by bacteria such as *Staphylococcus aureus* (*S. aureus*, Gram-positive), *Escherichia coli* (*E. coli*, Gram-negative), and *Pseudomonas aeruginosa* (*P. aeruginosa*). These infections frequently cause symptoms including redness, swelling, wound dehiscence, and increased pain. We evaluate the antimicrobial effects of wood woundplast on those bacteria by using the inhibition zone method. The diameters of the bacteriostatic zones of different samples are then quantified. As shown in Figure 4A, wood woundplast shows no antibacterial effect on any of the three bacteria when its concentration is 1 $\mu g \cdot mL^{-1}$. Curcumin induces dose-dependent expansion of inhibition zones across all three bacterial strains, with diameters increasing from 11.25 mm, 12.33 mm, 11.33 mm at 10 $\mu g \cdot mL^{-1}$ to 15.80 mm, 19 mm, 17.50 mm at 100 $\mu g \cdot mL^{-1}$ and 24.60 mm, 24.00 mm, 24.75 mm at 500 $\mu g \cdot mL^{-1}$. A maximum inhibition zone diameter of 33.75 mm, 27.33 mm, and 31.67 mm is achieved at 1000 $\mu g \cdot mL^{-1}$, suggesting that antimicrobial efficacy reaches a plateau at this concentration. Escalating to 2000 $\mu g \cdot mL^{-1}$ counterintuitively reduces inhibition zone diameters by 11.11%, 2.41%, and 1.07%, indicating that 1000 $\mu g \cdot mL^{-1}$ represents the optimal antimicrobial concentration. The inhibition effect of 1000 $\mu g \cdot ml^{-1}$ curcumin on *E. coli*, *S. aureus*, and *P. aeruginosa* is 3.07, 2.56, and 2.97 times higher than that of 1 $\mu g \cdot ml^{-1}$. Comparative SEM analysis of bacterial morphologies on material surfaces further validated the antibacterial efficacy of wood hydrogel-1000 (WH-1000). The surfaces of wood hydrogel-1 (WH-1) exhibit dense populations of structurally intact bacteria with preserved cellular morphology, while WH-1000 surfaces show complete absence of morphologically identifiable bacteria (Fig. 4C). This eradication of surface-colonizing bacteria demonstrates the capacity of WH-1000 to disrupt bacterial viability.

An ideal wound dressing should have both low cytotoxicity and absorption capacity. In order to verify the cytotoxicity of wood woundplast, we tested curcumin, PVA, and WH-1000 using the CCK-8 assay with RAW 264.7 cells as a representative cell line (Fig. 4D). These results indicate that the samples are nontoxic to cells. Water repellency angle testing confirms the superhydrophilic properties of wood woundplast, indicating good liquid absorption capabilities (Fig. S9). Although curcumin shows excellent anti-inflammatory effects in clinical settings, the anti-inflammatory effects of wood woundplast still need evaluation. Real-time fluorescence quantitative RT-PCR (RT-qPCR) is used to detect the expression levels of three inflammatory factors, including IL-1β, IL-6, and TNF-α (the relevant primer sequences are summarized in Table S1). Wood woundplast exudate is collected and evaluated using the same method as the CCK-8 test. After LPS induction, the expression levels of all three inflammatory genes are significantly increased among RAW 264.7 cells compared to the control group. Quantitative analysis reveals that wood woundplast significantly suppresses pro-inflammatory cytokine expression compared to LPS-stimulated controls: IL-1β decreased by 95.38%, IL-6 by 89.28%, and TNF-α by 99.736%. This obverse reduction in inflammatory markers demonstrates the capacity of wood woundplast to deliver localized anti-inflammatory effects at wound sites (Fig. 4E). Combined antimicrobial and anti-inflammatory properties, the wood woundplast can effectively accelerate wound healing.

3.4 Wound healing performances

Wound healing is a dynamic process influenced by various factors such as wound size, infection, and physiological state, which typically progresses through four consecutive stages, including hemorrhage, inflammatory response, tissue proliferation, and remodeling. After the initial hemorrhage response, the inflammatory phase (0–3 days) commences. Neutrophils and macrophages rapidly migrate to the wound site to phagocytose pathogens and clear cellular debris. Blood vessels dilate and become more permeable, leading to wound edema and the formation of fibrin clots around the wound periphery. Wood woundplast effectively absorbs wound exudate while releasing curcumin particles, which reduces inflammatory factors (IL-1β, IL-6, TNF-α, and so on) production and prevents excessive inflammation. The proliferative phase (days 3–10) follows, during which fibroblasts proliferate and produce collagen to form granulation tissue. Curcumin is continuously released

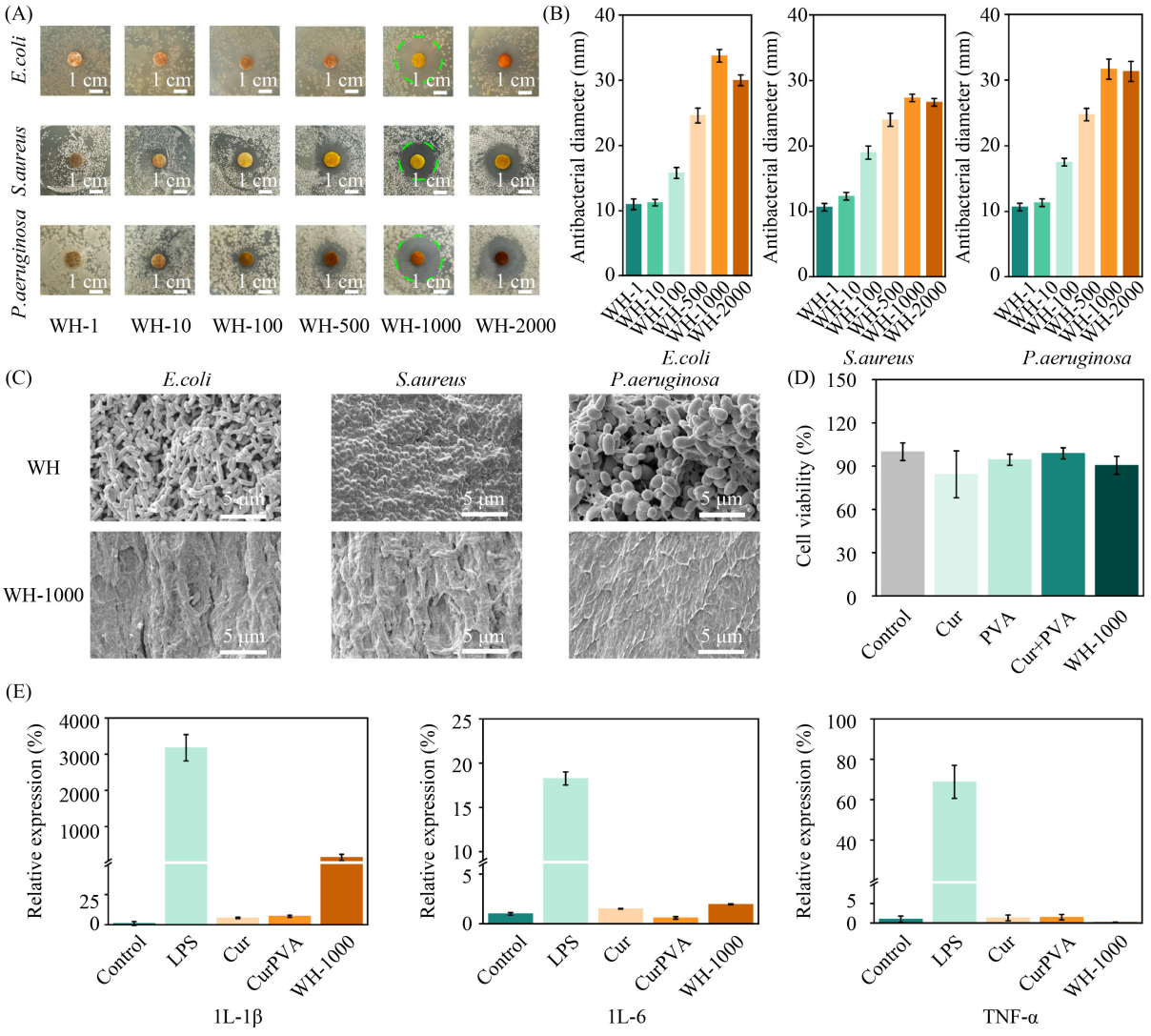

Fig. 4 Antimicrobial, *in vitro* cytotoxicity, and anti-inflammatory efficacy of wood woundplast. (A) Antimicrobial activity of WH with different curcumin concentrations on *E. coli, S. aureus,* and *Pseudomonas aeruginosa* in the disk diffusion assay. WH-1, WH-10, WH-100, WH-500, WH-1000, WH-2000, where "1, 10, 100, 500, 1000, 2000" represent curcumin concentrations, unit: $\mu g \cdot ml^{-1}$. (B) Quantified inhibition diameters of bacteriostatic zones of *E. coli, S. aureus,* and *Pseudomonas aeruginosa*, respectively. (C) SEM images of *E. coli*, *S. aureus,* and *Pseudomonas aeruginosa* on the surface of WH-1 and WH-1000. (D) Cell viability of fibroblasts cocultured with different samples or normal cell culture medium for 48 h. (E) RT-qPCR analysis of mRNA expression of IL-1β, IL-6, and TNF-α in RAW 264.7 cells after LPS induction.

throughout this phase, stimulating fibroblast activity and promoting collagen synthesis. Concurrently, keratinocytes at the wound margins proliferate and migrate to re-epithelialize the defect, while myofibroblasts actively contract to reduce wound defects, enhancing wound healing. During the remodeling phase (> 10 days), collagen fibers mature and realign, blood vessels regress with stabilized perfusion, scarring begins, and skin appendages such as hair follicles start to regenerate (Fig. 5A). Furthermore, moisture management in wound dressings plays a critical role in the wound healing process. A dressing with excessively high moisture permeability [water vapor transmission rate (WVTR) > 2000 $g \cdot m^{-2} \cdot d^{-1}$] tends to cause dry scab formation [47,48], while excessively low permeability may lead to wound maceration. Compared with commercial cotton (WVTR of 2691 $g \cdot m^{-2} \cdot d^{-1}$) and gauze (WVTR of 2461 $g \cdot m^{-2} \cdot d^{-1}$), wood woundplast exhibits a lower WVTR of 1591 $g \cdot m^{-2} \cdot d^{-1}$ (Fig. S11), which prevents excessive water vapor transmission and dry scab formation. At the same time, its WVTR is higher than the transepidermal water loss rate of intact skin, enabling maintenance of a moist wound environment with adequate breathability. It is suitable for

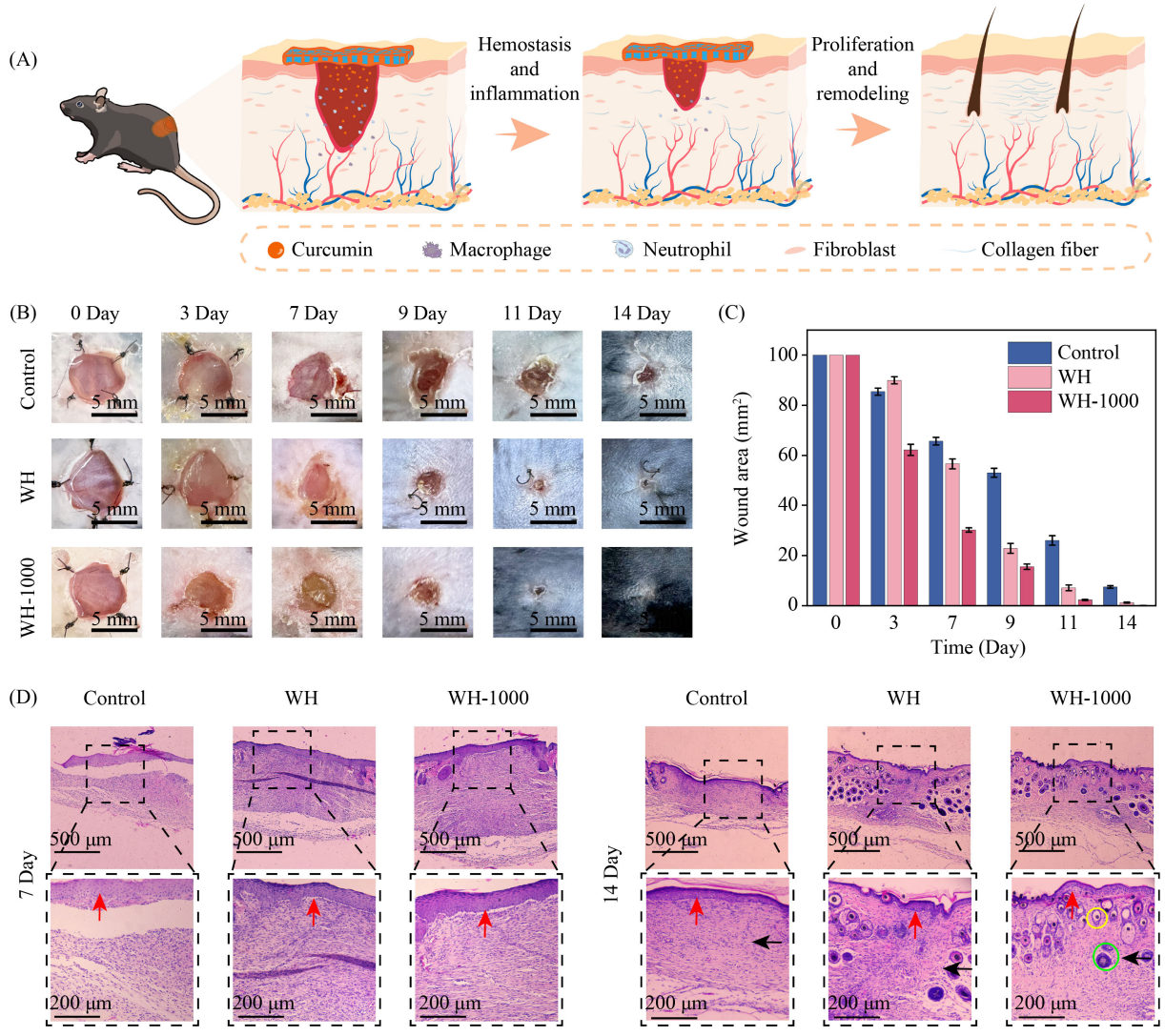

Fig. 5 *In vivo* wound healing efficacy of wood woundplast. (A) Schematic of the chronic wound healing process under the action of wood woundplast. (B) Representative photographic images of wounds in different groups (control, WH, and WH-1000 groups) after 0, 3, 7, 9, 11, and 14 days of treatment. (C) Quantification of wound area in each group. (D) Images of H&E staining of wounds in different groups on day 7 and day 14. The black arrow points to the wound healing site, the red arrow points to the dermis, the yellow circle is the hair follicle, and the green circle indicates the sebaceous gland.

wounds with low to moderate exudate levels.

We created a standardized full-thickness wound model (6 mm diameter) on the shaved backs of mice to evaluate the effects of wood woundplast on wound healing. Prior to surgery, hair was removed using depilatory cream, followed by thress complete cycles of alternating iodine and alcohol disinfection to minimize local irritation. Identical circular wounds were made in all three groups (blank, control, and experimental) using the same methodology. The wounds were then treated with control, WH, and wood woundplast, respectively, with dressings changed daily. Wound healing images analysis reveals that wood woundplast significantly accelerated tissue repair. During the late inflammatory phase (day 3), the wood woundplast group showed accelerated healing with a healing rate of 37.78%, significantly higher than that of the WH group (10.06%) and the control group (14.56%). The latter two groups exhibited no significant change in wound size at this stage (Fig. 5B). The early healing effects of wood woundplast stem from curcumin release, which prevents bacterial invasion and reduces the production of inflammatory factors. By the proliferative phase (day 7), the wood woundplast achieved a healing rate of 69.82%, which is twice that of the control group (34.28%) and 1.6 times that of the WH group (43.40%) (Fig. 5B, C). Hematoxylin and eosin (H&E) staining confirmed significantly greater epithelial coverage in wood woundplast compared to controls (Fig. 5D). This

improvement is attributable to superior exudate management of wood woundplast, which reduces bacterial burden and secondary inflammation. By the early remodeling phase (day 11), the wood woundplast group achieves a healing rate of 97.72% with the wounds completely healed at day 14. At day 14, wounds in the WH group showed only 1.24% unhealed area, while the control group retained 7.48% unhealed tissue. The wood woundplast enhances healing quality, as evidenced by day 14 histology exhibited complete regeneration of stratified epithelium, mature granulation tissue, and fully developed hair follicles and sebaceous glands (Fig. 5D). In contrast, the WH group displayed immature adnexal structures, and the control group showed no new hair follicles or sebaceous glands. Additionally, wood woundplast adhered to the skin and adapts to bending and deformation (Fig. S10). These results demonstrate that wood woundplast not only significantly accelerates the wound closure but also promotes high-quality tissue repair, including the regeneration of skin appendages.

4 Conclusion

In this study, we have prepared a flexible wood woundplast via a top-down approach. The deep eutectic solvent delignification treatment partially removes lignin and hemicellulose from natural wood, thereby creating a porous structure. This preservation of the inherent three-dimensional porous scaffold of the wood results in significantly enhanced flexibility. The curcumin is combined with highly hydrating polyvinyl alcohol (PVA) and encapsulated within the wood porous structure to form a cross-linked network structure. Benefiting from the strong hydrogen bonding between cellulose and PVA, the wood woundplast exhibits excellent mechanical properties, including a tensile strain of up to 270% and remarkable fatigue resistance, enduring over 300 tensile stress cycles without structural failure. The incorporation of curcumin endows the wood woundplast with significant antibacterial and anti-inflammatory functions. This dual functionality is achieved through bacterial membrane disruption (effective against *E. coli*, *S. aureus*, and *P. aeruginosa*) and suppression of pro-inflammatory cytokines (e.g., IL-1β, TNF-α, and IL-6), all while maintaining excellent cytocompatibility. Importantly, *in vivo* animal wound healing experiments demonstrate that the wood woundplast effectively shortens both the inflammatory and proliferative phases, significantly accelerating the wound healing process. Derived from natural wood and plant extracts, this material demonstrates significant potential to accelerate wound healing while providing both antibacterial and anti-inflammatory benefits, holding promising applications in trauma dressings, chronic wound management, and smart healthcare fields.

Supporting Information Supporting Information is available in the online version of this article at https://doi.org/10.2738/ENGB.2026.0002 and is accessible for authorized users.

Data Availability The data that support the findings of this study are available from the corresponding author upon reasonable request.

Acknowledgements This work was supported by the National Natural Science Foundation of China (32371790), the Fundamental Research Funds for the Central Universities (2572025JT02), the Key R&D Program of Heilongjiang Province (2024ZXDXC28), the China Postdoctoral Science Foundation (2020M681067), and the Special Funding Project of Postdoctoral in Heilongjiang Province (LBH-TZ2001). The authors used DeepSeek, online version as a language-editing tool to improve grammar, clarity, and readability. The AI tool was not used for data analysis, data generation, image processing, or scientific content creation. All outputs were carefully reviewed and verified by the authors, who take full responsibility for the final content.

Competing interests The authors declare no conflicts of interest.

Compliance with ethics guidelines All animal experiments were conducted in accordance with the Guide for the Care and Use of Laboratory Animals and were approved by the Science and Technology Ethics Committee of Northeast Forestry University (Approval No. 2025071). All efforts were made to minimize animal suffering.

References

1. Falanga V, Isseroff R R, Soulika A M, et al. Chronic wounds. Nature Reviews Disease Primers, 2022, 8(1): 50
2. Mostafalu P, Tamayol A, Rahimi R, et al. Smart bandage for monitoring and treatment of chronic wounds. Small, 2018, 14(33): 1703509
3. Chen D D, Tan G X, Tian S H, et al. Advancements in nanozymes research for the management of chronic wounds. Chemical Engineering Journal, 2024, 500: 157299
4. Miranda-Calderon L, Yus C, Remirez de Ganuza C, et al. Combinatorial wound dressings loaded with synergistic antibiotics in the treatment of chronic infected wounds. Chemical Engineering Journal, 2023, 476: 146679
5. Liang Y P, He J H, Guo B L. Functional hydrogels as wound dressing to enhance wound healing. ACS Nano, 2021, 15(8): 12687−12722
6. He L, Liu Y Z, Song P P, et al. Efficient photothermal, flexible wood-based hydrogel for infected wound recovery. ACS Sustainable Chemistry & Engineering, 2023, 11(33): 11529−11540
7. Jia B, Li G W, Cao E T, et al. Recent progress of antibacterial hydrogels in wound dressings. Materials Today Bio, 2023, 19: 100582
8. Hu B, Gao M Z, Boakye-Yiadom K O, et al. An intrinsically bioactive hydrogel with on-demand drug release behaviors for

diabetic wound healing. Bioactive Materials, 2021, 6(12): 4592−4606
9. Li Y, Hao D F, Feng G, et al. A hydrogel wound dressing ideally designed for chronic wound care. Matter, 2023, 6(4): 1060−1062
10. Xu D, Feng Y H, Song M J, et al. Smart and bioactive electrospun dressing for accelerating wound healing. Chemical Engineering Journal, 2024, 496: 153748
11. Zhang X Y, Wu Y, Gong H, et al. A multifunctional herb-derived glycopeptide hydrogel for chronic wound healing. Small, 2024, 20(36): 2400516
12. Feng F, Zhao Z H, Li J W, et al. Multifunctional dressings for wound exudate management. Progress in Materials Science, 2024, 146: 101328
13. Xu B, Li A, Wang R, et al. Elastic Janus film for wound dressings: unidirectional biofluid transport and effectively promoting wound healing. Advanced Functional Materials, 2021, 31(41): 2105265
14. Geng H M, Zheng X Y, Zhang Y L, et al. Microenvironment‐responsive hydrogels with detachable skin adhesion and mild‐temperature photothermal property for chronic wound healing. Advanced Functional Materials, 2023, 33(51): 2305154
15. Zhang X Y, Liang Y P, Huang S F, et al. Chitosan-based self-healing hydrogel dressing for wound healing. Advances in Colloid and Interface Science, 2024, 332: 103267
16. Mao G Z, Tian S Y, Shi Y X, et al. Preparation and evaluation of a novel alginate-arginine-zinc ion hydrogel film for skin wound healing. Carbohydrate Polymers, 2023, 311: 120757
17. Tanrikulu I C, Dang L N, Nelavelli L, et al. Synthetic collagen hydrogels through symmetric self-assembly of small peptides. Advanced Science, 2024, 11(3): 2303228
18. Wu Y, Jia D X, Lu K Y, et al. Bacterial cellulose-based dressings with photothermal bactericidal activity and pro-angiogenic ability for infected wound healing. Journal of Materials Science & Technology, 2023, 160: 76−85
19. Meng X Z, Zhou J, Jin X, et al. High-strength, high-swelling-resistant, high-sensitivity hydrogel sensor prepared with wood that retains lignin. Biomacromolecules, 2024, 25(3): 1696−1708
20. Chen J Q, Chen J S, Zhu Z L, et al. Drug-loaded and anisotropic wood-derived hydrogel periosteum with super antibacterial, anti-inflammatory, and osteogenic activities. ACS Applied Materials & Interfaces, 2022, 14(45): 50485−50498
21. Hayashi K, Tokumaru T, Shibahara K, et al. Wood-derived hydrogels for osteochondral defect repair. ACS Nano, 2025, 19(1): 520−534
22. Zhang W, Zhai W X, Xu M, et al. Constructing reinforced flexible wood-based hydrogels leveraging the ordered structure of wood for potential wound treatment. ACS Sustainable Chemistry & Engineering, 2025, 13(15): 5689−5702
23. Baş Y, Berglund L, Niittylä T, et al. Preparation and characterization of softwood and hardwood nanofibril hydrogels: toward wound dressing applications. Biomacromolecules, 2023, 24(12): 5605−5619
24. Schubert M, Panzarasa G, Burgert I. Sustainability in wood products: a new perspective for handling natural diversity. Chemical Reviews, 2023, 123(5): 1889−1924
25. Luan Q, Zhang H, Chen C J, et al. Controlled nutrient delivery through a pH-responsive wood vehicle. ACS Nano, 2022, 16(2): 2198−2208
26. Huang S Q, Wang Z Y, Wu Q, et al. Top‐down assembly of photosensitizable flexible wood dressing with synergistic effect of anti‐infection and moisture management. Advanced Functional Materials, 2025, 35(26): 2423123
27. Li L Z, Shang Z Q, Tang J F, et al. Wood robot with magnetic anisotropy for programmable locomotion. Advanced Functional Materials, 2023, 33(6): 2207209
28. Wang S Z, Li H L, Xiao L P, et al. Unraveling the structural transformation of wood lignin during deep eutectic solvent treatment. Frontiers in Energy Research, 2020, 8: 48
29. Hong S, Shen X J, Yuan T Q, et al. Unlocking lignin's potential with innovative DES technology. Trends in Chemistry, 2023, 5(11): 827−839
30. Zeng Q K, Qi X L, Shi G Y, et al. Wound dressing: from nanomaterials to diagnostic dressings and healing evaluations. ACS Nano, 2022, 16(2): 1708−1733
31. He L, Liu Y Z, Chen F, et al. Flexible wood-based pH-responsive hydrogel excipient for rapid recovery of infected wounds. Reactive and Functional Polymers, 2023, 192: 105707
32. Guo B L, Liang Y P, Dong R N. Physical dynamic double-network hydrogels as dressings to facilitate tissue repair. Nature Protocols, 2023, 18(11): 3322−3354
33. Wang L R, Zhou M Y, Xu T L, et al. Multifunctional hydrogel as wound dressing for intelligent wound monitoring. Chemical Engineering Journal, 2022, 433: 134625
34. Canabal R, González-Bello C. Chemical sensors for the early diagnosis of bacterial resistance to β-lactam antibiotics. Bioorganic Chemistry, 2024, 150: 107528
35. Monahan C, Morris D, Nag R, et al. Risk ranking of macrolide antibiotics - Release levels, resistance formation potential and ecological risk. Science of the Total Environment, 2023, 859: 160022
36. Short F L, Lee V, Mamun R, et al. Benzalkonium chloride antagonises aminoglycoside antibiotics and promotes evolution of resistance. eBioMedicine, 2021, 73: 103653
37. Hettiarachchi S S, Perera Y, Dunuweera S P, et al. Comparison of antibacterial activity of nanocurcumin with bulk curcumin. ACS Omega, 2022, 7(50): 46494−46500
38. Gong Y, Wang P, Cao R, et al. Exudate absorbing and antimicrobial hydrogel integrated with multifunctional curcumin-loaded magnesium polyphenol network for facilitating burn wound healing. ACS Nano, 2023, 17(22): 22355−22370
39. Chen X, Zhang K, Liang J H, et al. Unleashing excellent antibacterial performance of natural rubber composites via herbal extracts. Composites Part B: Engineering, 2024, 272: 111171
40. Ma J Q, Du Z X, Gao S X, et al. Tea polyphenols-mediated supramolecular architectures: design and applications. Trends in Food Science & Technology, 2024, 152: 104665
41. Li D Y, Zhang C J, Gao Z S, et al. Curcumin-loaded macrophage-derived exosomes effectively improve wound healing. Molecular

Pharmaceutics, 2023, 20(9): 4453−4467
42. Chen C H, Chen L, Mao C Y, et al. Natural extracts for antibacterial applications. Small, 2024, 20(9): 2306553
43. Hussain Y, Alam W, Ullah H, et al. Antimicrobial potential of curcumin: therapeutic potential and challenges to clinical applications. Antibiotics, 2022, 11(3): 322
44. Zheng D T, Huang C X, Huang H H, et al. Antibacterial mechanism of curcumin: a review. Chemistry & Biodiversity, 2020, 17(8): e2000171
45. Chang Y, Wang Q, Huang J Q, et al. Curcumin-loaded bamboo shoot cellulose nanofibers: characterization and in vitro studies. Foods, 2023, 12(18): 3512
46. Hussein Y, Loutfy S A, Kamoun E A, et al. Enhanced anti-cancer activity by localized delivery of curcumin form PVA/CNCs hydrogel membranes: preparation and *in vitro* bioevaluation. International Journal of Biological Macromolecules, 2021, 170: 107−122
47. Rathore K, Upadhyay D, Verma N, et al. Asymmetric Janus nanofibrous agar-based wound dressing infused with enhanced antioxidant and antibacterial properties. ACS Applied Bio Materials, 2024, 7(11): 7608−7623
48. Yusof N L B M, Wee A, Lim L Y, et al. Flexible chitin films as potential wound-dressing materials: wound model studies. Journal of Biomedical Materials Research Part A, 2003, 66A(2): 224–232